Chemie der Erde 77 (2017) 429–441

Contents lists available at ScienceDirect

Chemie der Erde

journal homepage: www.elsevier.de/chemer

Original paper

Distribution of base metals and the related elements in the stream-sediments around the Ahar area (NW Iran) and their implications

Vartan Simmonds[a,*], Fatemeh Jahangiryar[b], Mohssen Moazzen[b], Ahmad Ravaghi[b,c]

[a] Research Institute for Fundamental Sciences, University of Tabriz, Tabriz, Iran
[b] Earth Sciences Department, University of Tabriz, Tabriz, Iran
[c] Geologic Survey of Iran-NW branch, Tabriz, Iran

ARTICLE INFO

Article history:
Received 28 July 2015
Received in revised form 9 May 2017
Accepted 13 July 2017
Editorial handling - M. Mansour Edraki

Keywords:
Ahar
Stream sediment
Base metals
Geochemical anomaly
Hydrothermal alteration
Cu-Au mineralization

ABSTRACT

The study area is located in the Ahar region, NW Iran. Volcanic rocks of Eocene cover major parts of the area, within which granitic-granodioritic intrusive bodies of Oligocene intruded and produced hydrothermal alterations and Cu-Au mineralization. This paper aims to explore anomalies of base metals and related elements across the region based on systematic sampling of stream sediments and using the secondary geochemical halos. In this regard, by taking into account factors such as stratigraphy, lithology, tectonics and the topologic center of the drainage system, 620 samples were taken from stream sediments and analyzed by Inductively Coupled Plasma Atomic Emission Spectroscopy (ICP-OES) method.

All the distinguished anomalies correlate well with Oligocene granitic-granodioritic rocks and the related hydrothermal alterations occurred within the Eocene andesitic-basaltic volcanics, especially at the NE part of the quadrangle, as well as with alterations within trachy-andesitic and andesitic volcanics of Pliocene at the SE part of the quadrangle, where epithermal gold and Pb-Zn mineralization is found. Most of he studied elements also show moderate to strong anomalies over the Sonajil porphyry-type Cu mineralization. Copper, and to some extent Mo, as well as Pb, Zn, Sn, W, As and Sb are the best examples of this association. Bismuth has more limited anomalies across the region, showing correlation with the granitoid intrusion at the east of Ahar and the hydrothermal alterations within the Pliocene andesitic and basaltic rocks at SE of Ahar quadrangle which, considering the presence of epithermal gold and Pb-Zn veins in both areas, can be attributed to epithermal processes. However, anthropogenic pollutions are also found for As, Fe, V, Ti, Ni and Co downstream the urban and rural areas. In this regard, besides the Sonajil area, where porphyry-type Cu mineralization is discovered, the NE and SE parts of the quadrangle present promising areas for further investigations.

1. Introduction

Among the surface materials important for studying secondary geochemical halos, stream-sediments have a significant place in small-scale and medium-scale investigations (Levinson, 1980). Geochemical surveys using multi-element analysis on stream sediments are widely used to describe the geochemical characteristics of a watershed, to identify areas with anomalous concentrations of elements (Cohen et al., 1999) and to discover potential ore deposits. Chemical composition of stream sediments tells important details about the lithology of the watershed and the presence of ore deposits and pollution sources (Rantitsch, 2000). This method is particularly applicable for watersheds with moderate precipitation rate.

In this regard, stream sediments surveys remain the general geochemical methodology used in regional reconnaissance exploration (e.g. for Au) in areas where relief permits development of distinct drainage systems (Hale and Plant, 1994; Fletcher, 1997). Sampling of stream sediments has advantage over the rock or soil sampling, as the latter represents only a relatively small area close to the sample site, while stream sediments in any part of a drainage system represent weathering products of the rocks present in the upper parts of the system. Such investigations are especially efficient in areas covered by alluviums and/or greenfields with limited rock outcrops. In this research, systematic sampling and analysis of stream sediments and statistical analysis of the obtained data

* Corresponding author at: Research Institute for Fundamental Sciences, University of Tabriz, 29 Bahman Boulevard, Tabriz, Iran.
E-mail addresses: simmonds_vartan@tabrizu.ac.ir, simmonds_vartan@yahoo.co.uk (V. Simmonds).

http://dx.doi.org/10.1016/j.chemer.2017.07.006
0009-2819/

are used to discover the potential anomalies of elements and so, the mineralized zones and promising areas across the 1:100000 quadrangle of Ahar.

The 1:100000 geologic map of Ahar covers an area of 3074 km^2, being located at NW Iran between latitudes of 47° N and 47° 30′ N and longitudes of 38° E and 38° 30′ E (Figs. 1 and 2). Based on structural-sedimentary classifications of Iran, this area is part of the Alborz-Azarbaidjan zone (Nabavy, 1976) and Central Iranian domain (Alavi, 1991; Agha Nabaty, 2004). Most of the area is covered by Tertiary magmatic rocks, especially Eocene andesitic-basaltic rocks of Urumieh–Dokhtar volcano-plutonic belt of Iran (UDMA, Fig. 1), which is formed by the subduction of Neo-Tethyan oceanic crust beneath the Central Iranian plate (Berberian and King 1981). The Eocene volcanic rocks across the UDMA are referred to as subduction-related normal arc calc-alkaline magmatic products (e.g., Berberian et al., 1982; Shahabpour, 2007; Ghorbani and Bezenjani, 2011; Moritz et al., 2016), representing the peak of magmatic activity across it (e.g., Stocklin, 1974; Alavi, 2004). If we consider the late Eocene-Oligocene age for the collision between Arabian and Iranian plates (e.g., Allen and Armstrong, 2008; Dargahi et al., 2010; Aghazadeh et al., 2011; Castro et al., 2013), the Oligocene and younger volcanic and intrusive rocks in NW Iran will coincide with collisional to post-collisional stage (e.g., Sungun porphyry stock, Alavi et al., 2014; Kighal porphyry stock, Simmonds, 2013; Sonajil porphyry stock, Hosseinzadeh et al., 2010).

Intrusion of granitic-granodioritic bodies of Oligocene age produced hydrothermal alteration halos and Cu and Au mineralization in the area (e.g., Sonajil porphyry-type Cu mineralization; Hosseinzadeh et al., 2010). By taking into account the potential of base metal mineralization across the region and the fact that subsequent weathering can release these metals from altered and mineralized rocks into the stream sediments, this study aims to determine the statistical relationships and geochemical characteristics of base metals and associated elements in stream sediments and to help identifying the likely sources of mineralization in the region.

2. Regional geology

Based on the 1:100000 geologic map of Ahar (Mahdavi and Amini Fazl, 1988), the oldest rock units in the area are volcanic and sedimentary rocks of upper Cretaceous. Volcanic units of this age are mainly comprised of porphyritic andesite, andesi-basalt and olivine basalt (K^v), accompanied and overlain by acidic pyroclastics (submarine volcanic breccia and tuffite) and sedimentary rocks, including basal conglomerate (unconformably overlying the volcanic rocks), sandstone, shale, marl (K^s) and micritic fossiliferous limestone (K^l), which have limited outcrops at west and northwest of the region.

About half of the region is covered by volcanic, intrusive and sedimentary rocks of Tertiary age (Fig. 2). Lithologic units of Paleocene-Eocene mainly include volcanic rocks formed in subaerial and subaqueous (shallow marine) conditions. Paleocene volcanic units include porphyritic andesite to trachy-andesite, tuff and agglomerate (P^v). Some sub-volcanic microdioritic and diabasic rocks also accompany this unit. Sedimentary rocks of Paleocene age (P^s) are comprised of alternations of gypsiferous marl, calcareous sandstone and thin-bedded light gray limestone, as well as a purple conglomerate containing volcanic pebbles, 2–15 cm diameter across, set in a completely consolidated matrix, which occupy small areas in the north and south of the Heris town (Fig. 2). Fossil species of *Radiolaria*, *Globigerinids* and *Globorotalids* indicate Paleocene to Lower Eocene ages.

Volcanic rocks of Eocene age cover most parts of the Ahar area, especially at its eastern section and include lava flows of porphyritic to mega-porphyritic andesite to trachy-andesite, pyroxene andesite and andesi-basalt compositions, which have experienced kaolinization and alunitization, trachy-andesitic to trachytic lavas with coarse crystals of secondary analsim, basic lavas of olivine basalt, andesi-basalt and pyroxene andesite compositions, along with pyroclastic rocks of intensely silicified and sericitized acidic tuff, welded and brecciated crystal and lithic tuffs and ignimbrites of dacitic to rhyodacitic composition, and tuffite (E^v). Some thin-bedded nummulite-bearing limestone lenses are also found confined within these volcanics, which indicate early to middle Eocene age (E^l).

Rock units of Oligocene age include scarce occurrences of rhyolitic domes (O^r), dacitic breccias and ignimbrite, and several large intrusive bodies, including Khankandi, Yuseflu, Sonajil and Razgah. The Khankandi pluton is comprised of granodiorite-quartz monzonite and monzonite-gabbro phases and lamprophyric and dacitic dikes, in order of emplacement (Jamali et al., 2012). Monzonites and gabbros form the main part of this pluton (Aghazadeh et al., 2010). Yuseflu pluton is composed of quartz monzonite, granodiorite and granite phases, later intruded by a non-altered and non-mineralized monzonitic stock (Jamali et al., 2012). Both these plutons are tectonically post-collisional (Jamali et al., 2012). The Sonajil intrusive complex includes a porphyritic microdioritic stock (the host of porphyry-type Cu mineralization) and a dioritic to quartz-dioritic body (known as Incheh granitoid), in order of emplacement, which are emplaced within the pyroxene andesites, brecciated tuffs and ignimbrites of Eocene age during the post-collisional stage of the Neo-Tethys ocean closure (Hosseinzadeh et al., 2010).

Another body of monzosyenite to pseudoleucite-bearing monzosyenite (ms) is located at the southeast of Ahar quadrangle (Razgah area) with 15–20 km^2 surface area (Mahdavi and Amini Fazl, 1988), having indistinct contact with parts of Miocene units. Several other intrusive bodies of granitic to granodioritic composition have also outcropped in the area (Mahdavi and Amini Fazl, 1988). It must be noted that hydrothermal alterations in the study area are mainly related to Oligocene intrusive magmatism, which have mostly affected Eocene volcanic host rocks.

Miocene units are sedimentary, comprised of marliferous limestone, gypsiferous marl and gypsum with no fossil traces, as well as alternations of sandstone, siltstone and marl intercalated with thin-bedded fossiliferous (*gastropoda*) limestone (maximum thickness of 10 m) (M^s), which have mainly outcropped at the southern and southwestern parts of the Ahar quadrangle.

Pliocene is characterized by a red-colored basal conglomerate and sandy conglomerate (Pl^s), unconformably overlying sedimentary and submarine volcanic rocks of upper-Cretaceous and Eocene, as well as Miocene marls. Conglomerate is locally accompanied by thin red-colored gypsiferous marl layers. Additionally, outcrops of volcanic rocks, including rhyolitic to dacitic ignimbrite and andesitic to trachy-andesitic lavas are found at the southwest of the study area (Pl^v). In the SE part of the study area, Pliocene-Quaternary volcanic fumaroles have produced alterations within the surrounding rocks, particularly andesitic to trachy-andesitic lavas of Pliocene.

Plio-Pleistocene units are mainly found at the western part of the Ahar area, especially covering Ahar plain, and include weakly-sorted and rounded conglomerate, along with siltstone and layers of gypsum and purple-colored tuff. Additionally, lacustrine deposits comprised of gray bedded clay, marl, siltstone and fine-grained sandstone, accompanied by thin beds of microconglomerate to conglomerate are observed in the Heris plain (QPl^s).

Quaternary units include unconsolidated pebble-bearing alluvial fans with variable thicknesses reaching up to several meters and unconformably overlying Plio-Pleistocene sediments in some

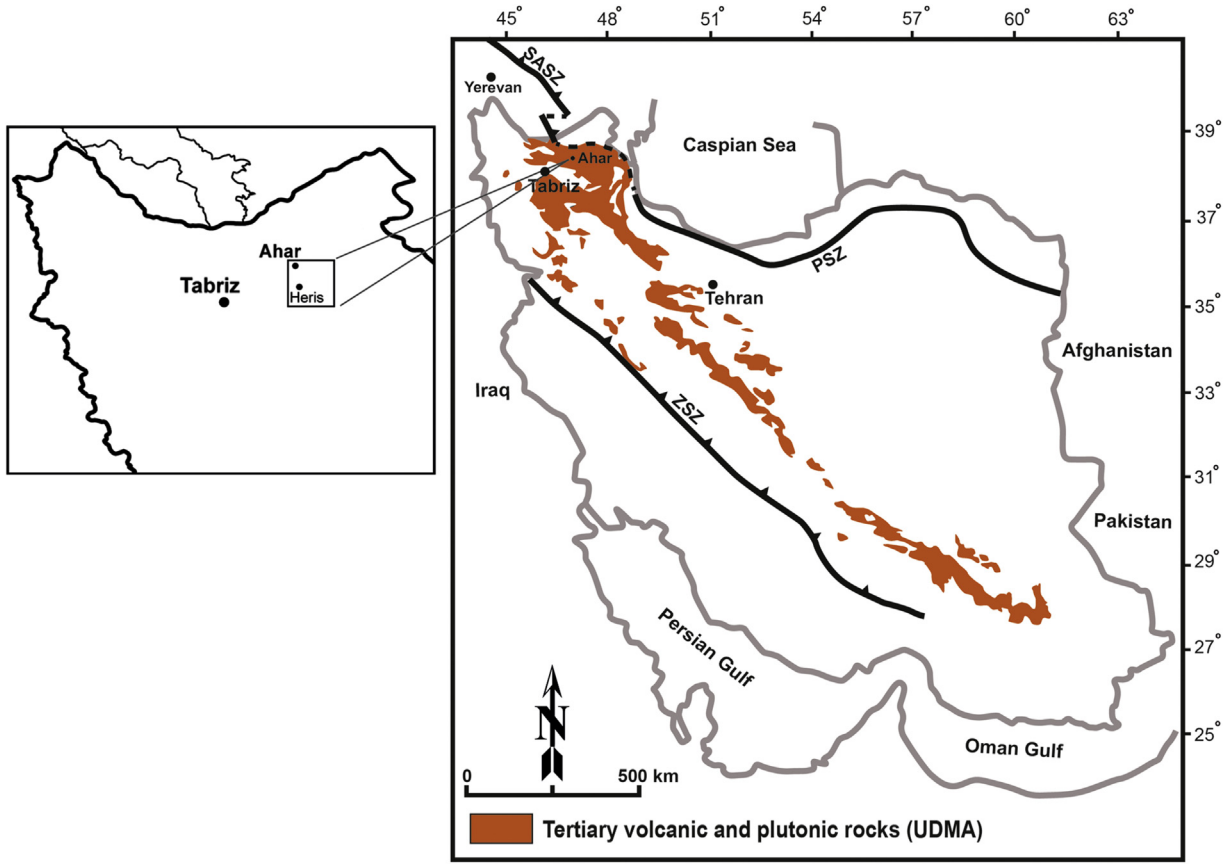

Fig. 1. The location of Ahar 1:100000 geologic map quadrangle in NW Iran. PSZ: Paleo-Tethys Suture Zone (Axen et al., 2001), ZSZ: Zagros Suture Zone (Agha Nabaty, 2004), SASZ: Sevan-Akera Suture Zone (Mederer et al., 2014). The location of Urumieh-Dokhtar magmatic arc from Agha Nabaty (2004).

places, alluvial sediments consisted of gravel and fine sand, which fill valleys of the main rivers, such as Ahar River and Talkherood, as well as salt and clay flats (Q) and finally, limited outcrops of basaltic lavas and related pumice occurrences, which overlay lacustrine deposits (Q^v).

2.1. Economic geology

A porphyry-type copper mineralization is occurred in the Sonajil area, east of Heris (Fig. 2). Furthermore, evidence of Cu mineralization is also found in monzosyenitic to pseudoleucite-bearing monzosyenitic body of Razgah, occurred as chalcopyrite, malachite and chalcocite. Meanwhile, the nepheline syenitic rocks of the Razgah intrusive body are exploited for alumina production (Fig. 2).

Another mineral occurrence in the area with high economic value is alunite, which has hydrothermal origin, being found as alunitic alteration zones, which are much wider at the northeast of the Ahar area (Zaylik area).

Finally, percolation of hydrothermal fluids within andesitic to trachy-andesitic rocks at the north and east of the area is brought about kaolinization and formation of kaolinite occurrences.

3. Materials and methods

3.1. Sampling and geochemical analysis

In order to carry out stream sediment investigation across the Ahar area, a sampling network was designated considering the stratigraphic, lithologic and tectonic characteristics of the area. The sampling density was considered higher around the intrusive bodies and their contacts, at the vicinity of faults and their intersection zones, hydrothermally altered zones and areas overlying the intrusive and sub-volcanic bodies (identified over aerial geophysical map) (Hassani Pak and Sharafaldin, 2005). Another issue which must be considered was anomalies arisen from agricultural activities in the vicinity of river and stream banks with rather flat topography. The problem is that application of chemical fertilizers may produce anomalies of rare earth elements in the down-stream sediments (Hassani Pak and Sharafaldin, 2005; Nude and Arhin, 2009). Urban and rural areas also produce bio-environmental pollutions. In this regard, it was attempted to take samples from up-streams of the agricultural fields. Considering the above-mentioned factors, the density of sampling network varied from 1 sample per km^2 to 1 sample per 50 km^2, with an average of 1 sample per 3–4 km^2 in arid parts to 1 sample per 5–6 km^2 in wet parts of the study area.

Geochemical sampling was conducted across the 1:100000 geologic map of Ahar by taking 620 stream sediment samples from the depth of 25–30 cm at each point, drying and sieving them (−80 mesh size; <0.177 mm) to get ~200 g fine-grain sample. After transferring to laboratory, samples were dried at 80 °C in oven for about an hour, crushed using jaw crusher and then roller crusher to achieve a homogeneous sample with particle sizes below 1 mm and finally pulverized using ball mill up to 200 mesh size (0.074 mm).

The obtained powders were dissolved using 10 ml of HF and 3 ml of $HClO_4$ and then by 10 ml of aqua regia and were analyzed for 44 elements by Inductively Coupled Plasma Atomic Emission Spectroscopy (ICP-OES) method using Varian-735 ES equipment in Applied Geological Research Center of Iran (GRCIR; Tehran). Instrument calibration was done using GBW07162 (GSO-1) certified

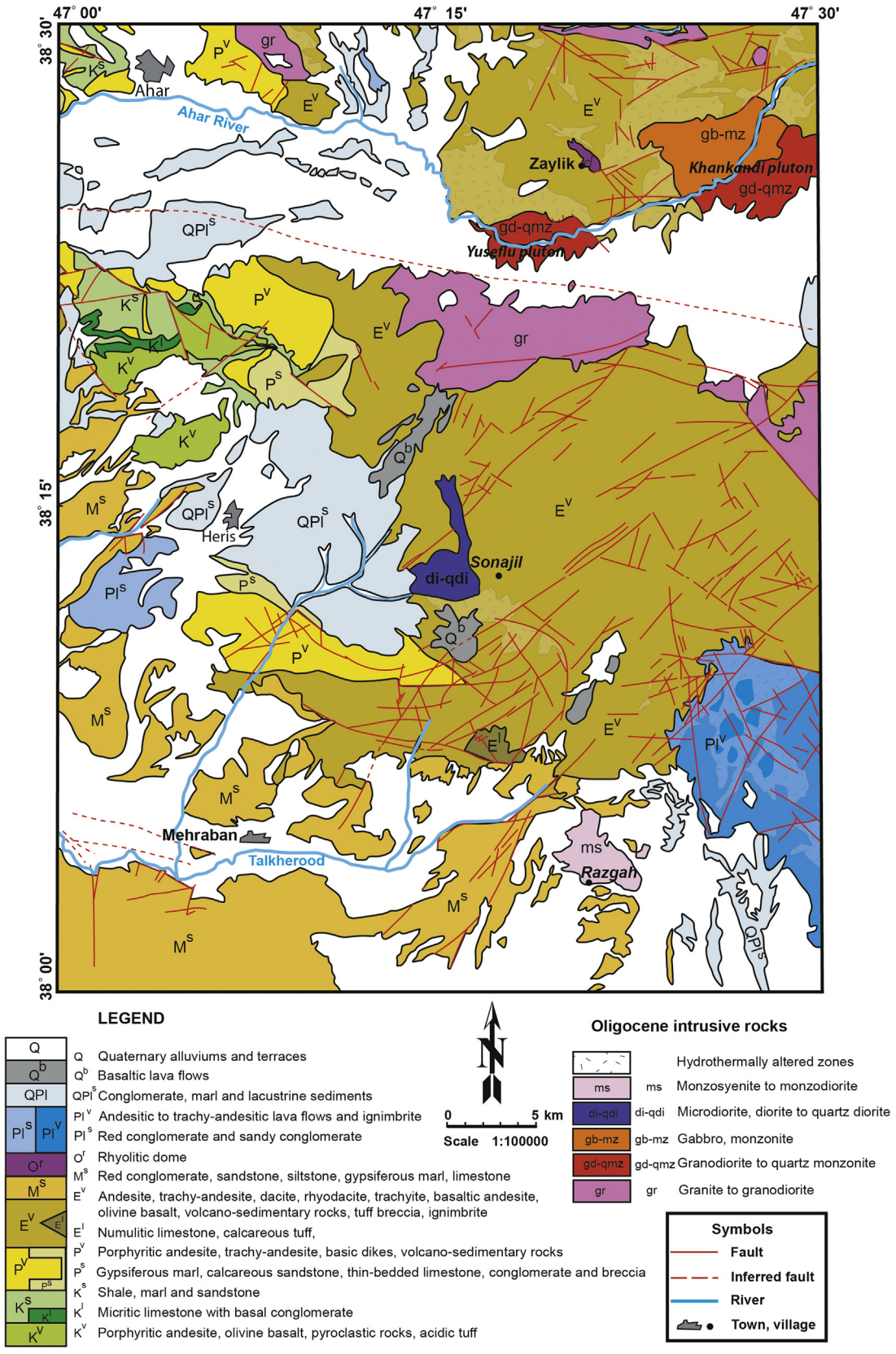

Fig. 2. 1:100000 geologic map of Ahar (simplified after Mahdavi and Amini Fazl, 1988).

multi-metal ore reference material, provided by Beijing Standard Material Center (Beijing, China). The uncertainty levels were about ±1% for the major oxides and about ±5% for minor and trace elements.

The gold content of the samples was determined by Fire Assay method at the GRCIR. For this, 30 g of each sample mixed with PbO, $NaCO_3$, $Na_2B_4O_7$, SiO_2 and a reducing agent was fused in the furnace at 950 °C. Then, the obtained Pb button was separated from the

Table 1
Statistical parameters of the raw data for the selected elements.

	Cu	Mo	Pb	Zn	Sn	W	As	Sb	Bi	Fe	Ti	V	Ni	Co	Mn
N Sample number	620	620	620	620	620	620	620	620	620	620	620	620	620	620	620
Mean	66.9	10.7	19.7	84.8	1.6	3.8	28.9	2.9	0.2	59110.6	6202.3	193.4	34.6	17. 9	1016.4
Median	60.3	2.6	17	81.6	1.5	2.9	19.8	2	0.2	56150	5940	176	28	16.7	1015
Mode	50.2	0.9	14.9	101	1.4	1.5	15.9	1.9	0.2	49300	5540	141	26	16.9	1020
Std. Deviation	36	135. 5	12	22.7	0.6	3.2	52.8	4	0.3	21651.4	1896	84.5	24.3	5.4	255.7
Variance	1299.4	18348.3	144	514.8	0.3	10.6	2786.7	16.4	0.09	4.7	3594655.8	7135.9	590.8	29.6	65376.5
Skewness	4.5	24.3	2.1	1.2	1.3	4	12.8	8.1	9.3	3.4	2	3	3	1.1	0.5
Std. Error of Skewness	0.1	0.1	0.1	0.1	0.1	0.1	0.1	0.1	0.1	0.1	0.1	0.1	0.1	01	0.1
Kurtosis	34.2	599.5	6. 8	3.1	4.4	27.8	212	86.3	135.4	22.8	8.9	17.9	13.9	1.5	2.9
Std. Error of Kurtosis	0.2	0.2	0.2	0.2	0.2	0.2	0.2	0.2	0.2	0.2	0.2	0.2	0.2	0.2	0.2
Minimum	22.5	0.3	1.1	31.8	0.5	0.6	1.5	0.2	0.1	20800	2280	64	5	6.2	255
Maximum	420	3350	91.9	202	5.1	37.2	1010	53.2	5.2	256000	21600	968	221	41.5	2460
Sum	41501.2	6622.5	12242.9	52610	991.4	2374.2	17931.9	1776.3	148.3	36648600	3845460	119917	21480	11094.2	630170

Table 2
Statistical parameters of the logarithmically normalized data for the selected elements (after omitting the out of range samples).

		Cu	Mo	Pb	Zn	Sn	W	As	Sb	Bi	Fe	Ti	V	Ni	Co	Mn
Sample No	Valid	611	596	606	616	620	609	590	600	608	611	611	612	608	618	618
	Out of Range	9	24	14	4	0	11	30	20	12	9	9	8	12	2	2
Mean		4.1	0.9	2.8	4.4	0.4	1	2.9	0.6	−1.8	10.9	8.7	5.2	3.3	2.8	6.9
Median		4.1	0.9	2.8	4.4	0.4	1	2.9	0.6	−1.6	10.9	8.7	5.2	3.3	2.8	6.9
Mode		3.9	−0.1	2.7	4.6	0.3	0.4	2.8	0.6	−1.6	10.8	8.6	4.9	3.3	2.8	6.9
Std. Deviation		0.4	0.8	0.5	0.2	0.3	0.6	0.6	0.7	0.6	0.3	0.3	0.3	0.5	0.3	0.3
Variance		0.1	0.6	0.3	0	0.1	0.4	0.4	0.5	0.4	0.1	0.1	0.1	0.3	0.1	0.1
Skewness		0.1	0	−0.6	0	0	0	−0.4	−0.6	0.2	0	−0.1	0.1	0	0.2	−1.1
Std. Error of Skewness		0.1	0.1	0.1	0.1	0.1	0.1	0.1	0.1	0.1	0.1	0.1	0.1	0.1	0.1	0.1
Kurtosis		−0.1	−0.5	1.6	1	0.2	−0.5	0.3	0.8	−0.7	0.4	0.8	0.2	−0.1	0.3	3.1
Std. Error of Kurtosis		0.2	0.2	0.2	0.2	0.2	0.2	0.2	0.2	0.2	0.2	0.2	0.2	0.2	0.2	0.2
Minimum		3.1	−1.2	0.1	3.5	−0.7	−0.5	0.4	−1.6	−2.6	9.9	7.7	4.2	1.6	1.8	5.5
Maximum		5.1	3.2	4	5.1	1.6	2.5	4.3	2.2	0.5	11.7	9.4	6.1	4.6	3.6	7.5
Sum		2500.8	552.1	1695.9	2711.9	254.8	658.5	1711.7	379.2	−1068.3	6673.1	5303.5	3169.2	2030.4	1754.9	4256.2

slag and placed in the pre-heated cupel at 950 °C, which led to the absorption and removal of Pb and left Au and Ag as a prill. The weighed prill was treated with HNO_3 to dissolve and remove Ag. The resultant Au prill was treated with HCl to dissolve Au. Gold concentration was measured using Varian 240FS atomic absorption spectrometer equipped with graphite furnace.

From the analyzed elements, Cu, Mo, Pb, Zn, Sn, W, As, Sb, Bi, Fe, Ti, V, Ni, Co and Mn were selected for studying their distribution parameters and probable anomalies across the region.

Finally, after determining the anomalous zones, field control survey and rock sampling was carried out in these zones and about 84 rock samples were taken and analyzed by ICP-OES method (using Varian-735 ES equipment) at the GRCIR.

3.2. Statistical studies

The obtained geochemical data were processed by Microsoft Excel (2007) and SPSS 20 softwares. The censored data were replaced by numerical values following the simple replacement method as most of the major statistical techniques require a complete set of numerical and non-censored data; this method is applicable when the number of censored data is less than the 10% of total data. Values greater than the upper detection limit and those smaller than the lower detection limit were replaced by the four third and three forth of the upper and lower detection limits, respectively (Hassani Pak, 2012).

The first step in processing the geochemical data is studying the statistical parameters of each element, aiming to identify its distribution nature, which includes the calculation of statistical parameters such as mean, median, mode, standard deviation, variance, skewness and kurtosis (Clark, 1987). The calculated statistical parameters of the selected elements (based on the raw data) are provided in Table 1 and the frequency histograms of these elements and their P–P plots are displayed in Figs. 3 and 4, respectively. During examination of the raw data, some samples were recognized which stand at the upper and lower margins of the total data population, isolated from the main population (out of range data). Such data can be clearly identified by box plots. Box plots of the selected elements are shown in Fig. 5. Implementation of some statistical methods requires normalization of the distribution function of the studied variables and elimination of out of range samples. Therefore, the raw data must be normalized before implementing such methods (Hassani Pak, 2012). In this regard, after identifying and elimination of out of range data, the data were logarithmically (natural logarithm) normalized and the statistical parameters and frequency histograms of the normalized data were prepared (Table 2 and Fig. 6). To recognize any meaningful relationships among the variables (elements), Spearman and Pearson correlation coefficients were calculated using raw and normalized data (Table 3).

Due to the fact that each group of elements behave more or less similar in response to environmental conditions, recognizing the relationship and mutual genetic correlation among various elements can be used for better understanding the variations within geochemical environments. Cluster analysis is a multi-variant statistical method, which classifies elements based on the similarity of their variations. It may also help to find the actual groups of elements and reduce the density of the data. Considering the abovementioned facts, cluster dendrogram of the studied elements was prepared and showed in Fig. 7.

3.3. Preparing anomaly maps

There are various statistical techniques, which help to optimize the exploration projects and to reduce the expenses (Chork, 1991). Stream sediment-based geochemical explorations lead to prepara-

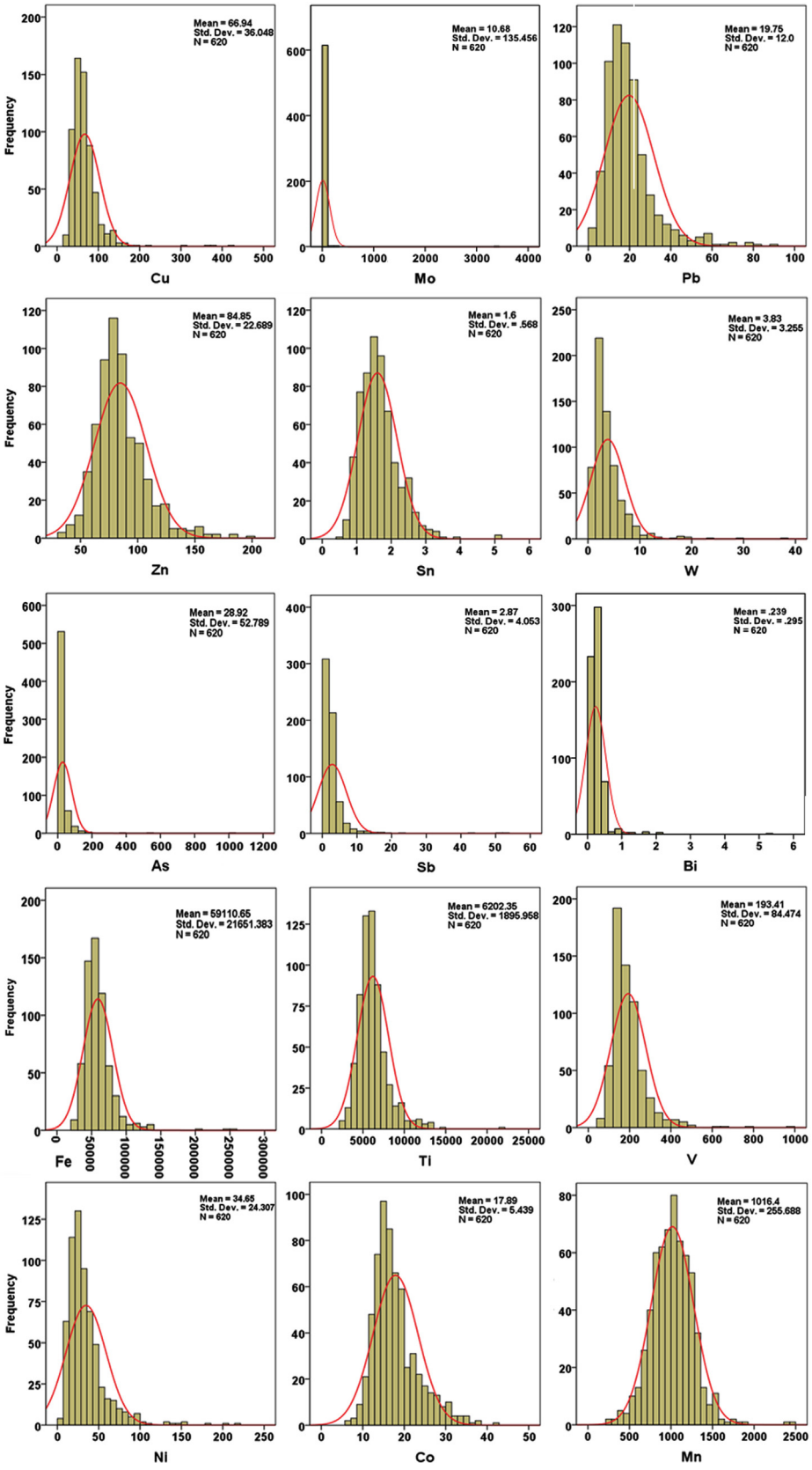

Fig. 3. Frequency histograms of the raw data for the selected elements.

tion of anomaly maps of elements, which have an important role in discovering the promising areas. The latter issue requires an appropriate and rational designation of the sampling network, precise sampling, efficient sample preparation and analyzing method with a defined and favorable error limit and finally an appropriate data processing (Chork, 1991). For the study region, the anomaly

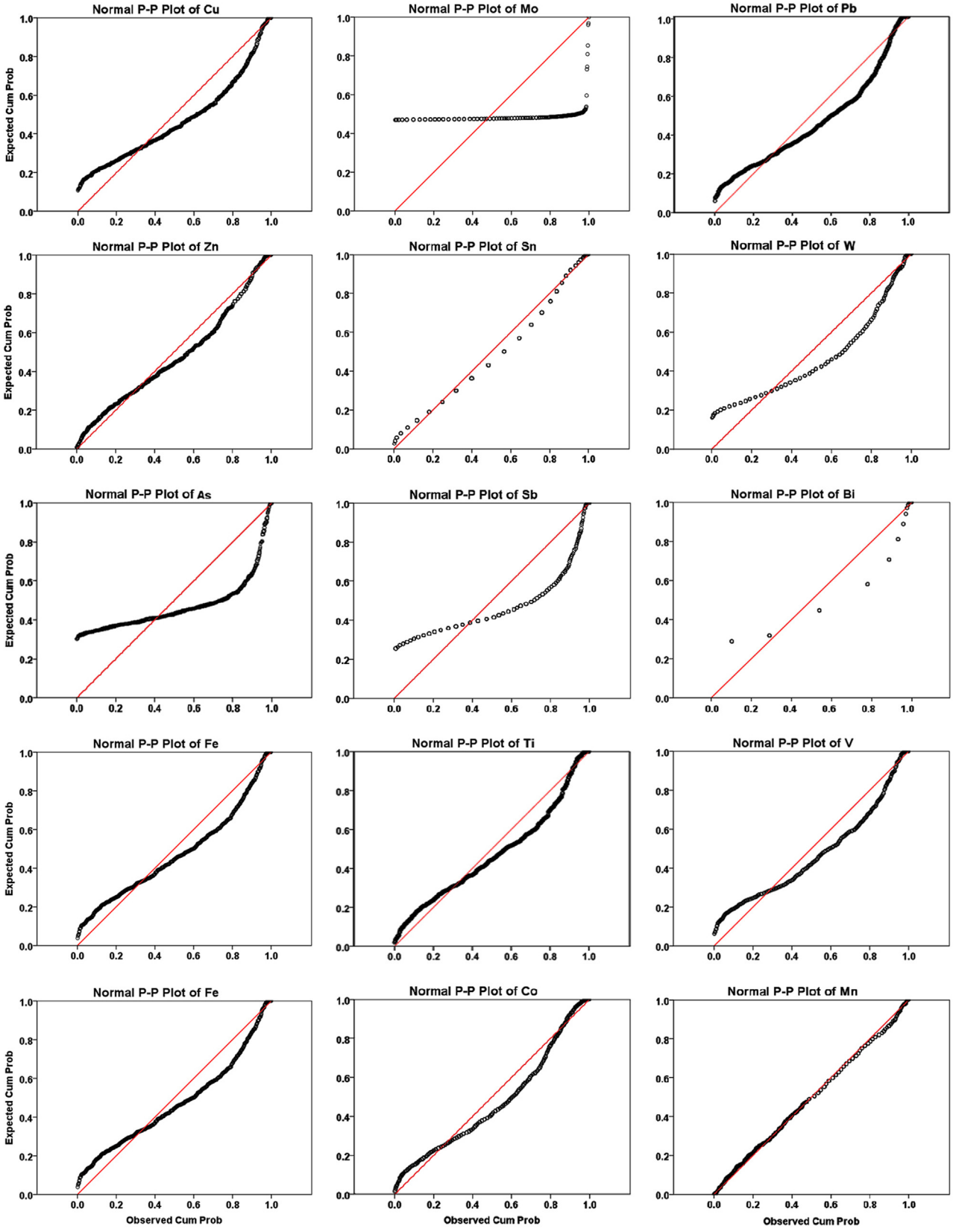

Fig. 4. Normal P–P plots of the raw data for the selected elements.

maps of elements were prepared based on Kriging method, using Surfer 8 software (Fig. 8). Kriging uses the data of sampling points to estimate the element concentration in not-sampled areas. Due to the large covering area of each sample in stream-sediment investigation and the low density of sampling in such environments, especially in similar investigations in Iran, this method has bet-

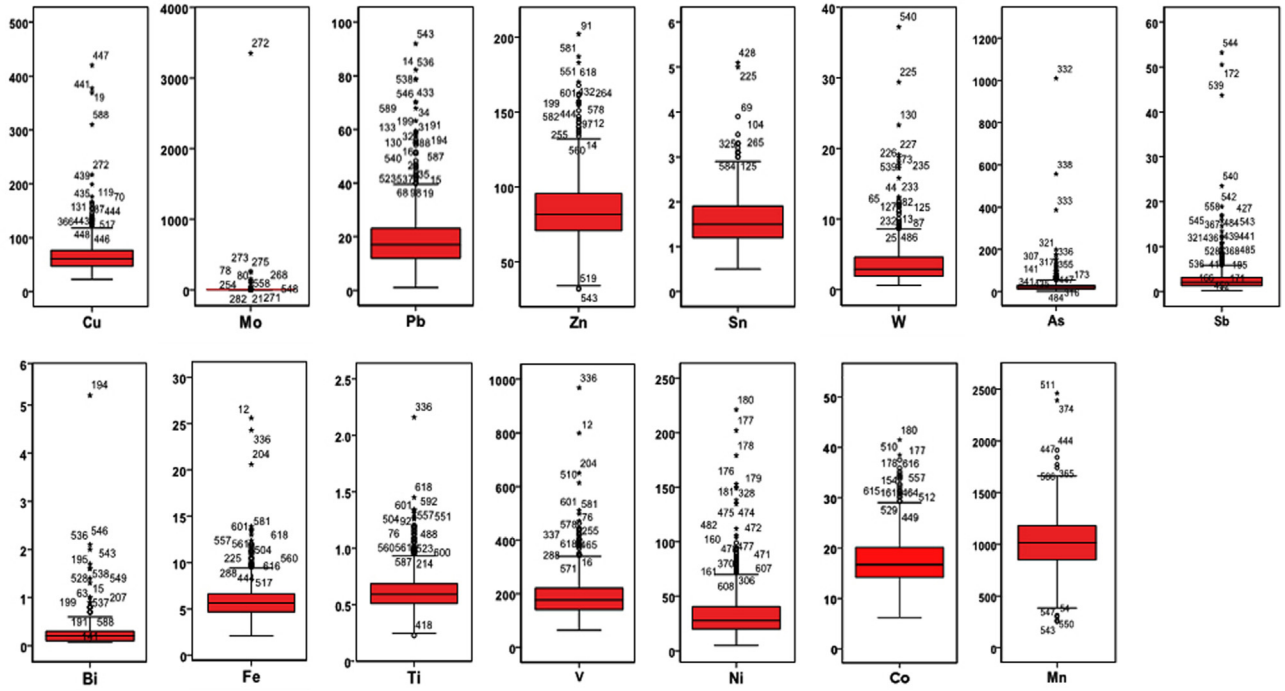

Fig. 5. Box-plots of the selected elements used to determine the out of range samples.

Table 3
(a) Spearman correlation coefficients between pairs of the selected elements using the raw data. (b) Pearson correlation coefficients between pairs of the selected elements using the normalized data.

(a)	Cu	Mo	Pb	Zn	Sn	W	As	Sb	Bi	Fe	Ti	V	Ni	Co	Mn
Cu	1.000														
Mo	−0.003	1.000													
Pb	0.216**	−0.529**	1.000												
Zn	0.371**	0.083*	0.408**	1.000											
Sn	0.055	0.398**	0.371**	0.272**	1.000										
W	0.152**	0.646**	0.689**	0.231**	0.483**	1.000									
As	0.005	0.325**	0.268**	0.069	0.295**	0.297**	1.000								
Sb	0.078	0.401**	0.473**	0.152**	0.306**	0.574**	0.597**	1.000							
Bi	−0.46	0.630**	0.599**	0.147**	0.458**	0.596**	0.457**	0.503**	1.000						
Fe	0.290**	−0.164**	−0.051	0.561**	0.082*	−0.030	−0.050	−0.056	−0.184**	1.000					
Ti	0.197**	0.092*	0.101*	0.503**	0.263**	0.208**	−0.032	0.034	−0.043	0.754**	1.000				
V	0.290**	−0.227**	−0.097*	0.509**	0.092*	−0.079*	−0.045	−0.051	−0.199**	0.929**	0.735**	1.000			
Ni	−0.185**	−0.127**	−0.252**	−0.093*	−0.041	−0.243**	−0.211**	−0.229**	−0.015	0.025	−0.115**	0.058	1.000		
Co	0.283**	−0.293**	−0.276**	0.385**	−0.250**	−0.246**	−0.208**	−0.153**	−0.272**	0.692**	0.419**	0.669**	0.342**	1.000	
Mn	0.394**	−0.170**	0.001	0.540**	−0.046	−0.052	−0.062	−0.113**	−0.205**	0.586**	0.382**	0.516**	−0.089*	0.588**	1.000

(b)	nCu	nMo	nPb	nZn	nSn	nW	nAs	nSb	nBi	nFe	nTi	nV	nNi	nCo	nMn
nCu	1.000														
nMo	0.171**	1.000													
nPb	0.222**	−0.031	1.000												
nZn	0.242**	−0.005	0.328**	1.000											
nSn	0.117**	−0.003	0.230**	0.275**	1.000										
nW	0.127**	−0.002	0.488**	0.228**	0.395**	1.000									
nAs	0.027	−0.008	0.028	0.018	0.084*	0.056	1.000								
nSb	0.055	−0.015	0.290**	0.110**	0.038	0.318**	0.195**	1.000							
nBi	0.055	0.004	0.514**	0.015	0.161**	0.231**	0.080*	0.218**	1.000						
nFe	0.113**	0.002	−0.065	0.577**	0.169**	0.050	0.038	−0.031	−0.066	1.000					
nTi	0.087*	0.004	0.018	0.550**	0.346**	0.155**	0.029	−0.035	−0.070	0.767**	1.000				
nV	0.126**	−0.070	−0.101*	0.548**	0.151*	−0.020	0.056	−0.026	−0.081*	0.954**	0.790**	1.000			
nNi	−0.110**	−0.004	−0.270**	−0.117**	−0.153**	−0.230**	−0.098*	−0.139**	−0.098*	0.053	−0.122**	0.053	1.000		
nCo	0.145**	−0.072	−0.284**	0.337**	−0.235**	−0.201**	−0.070	−0.113**	−0.178**	0.619**	0.398**	0.625**	0.512**	1.000	
nMn	0.246**	−0.014	−0.055	0.512**	0.026	0.026	0.010	−0.060	−0.203**	0.469**	0.374**	0.438**	0.027	0.549**	1.000

* Correlation is significant at the 0.05 level (2-tailed).
** Correlation is significant at the 0.01 level (2-tailed).

ter efficiency, compared with other methods (Hassani Pak and Sharafaldin, 2005). In such cases, raising the number of the cells with defined data will lead to revealing the logical relationship among the abundances of an element in various cells and provide the possibility to assess the existing distribution zoning of each element. For instance, if an anomaly is surrounded by background

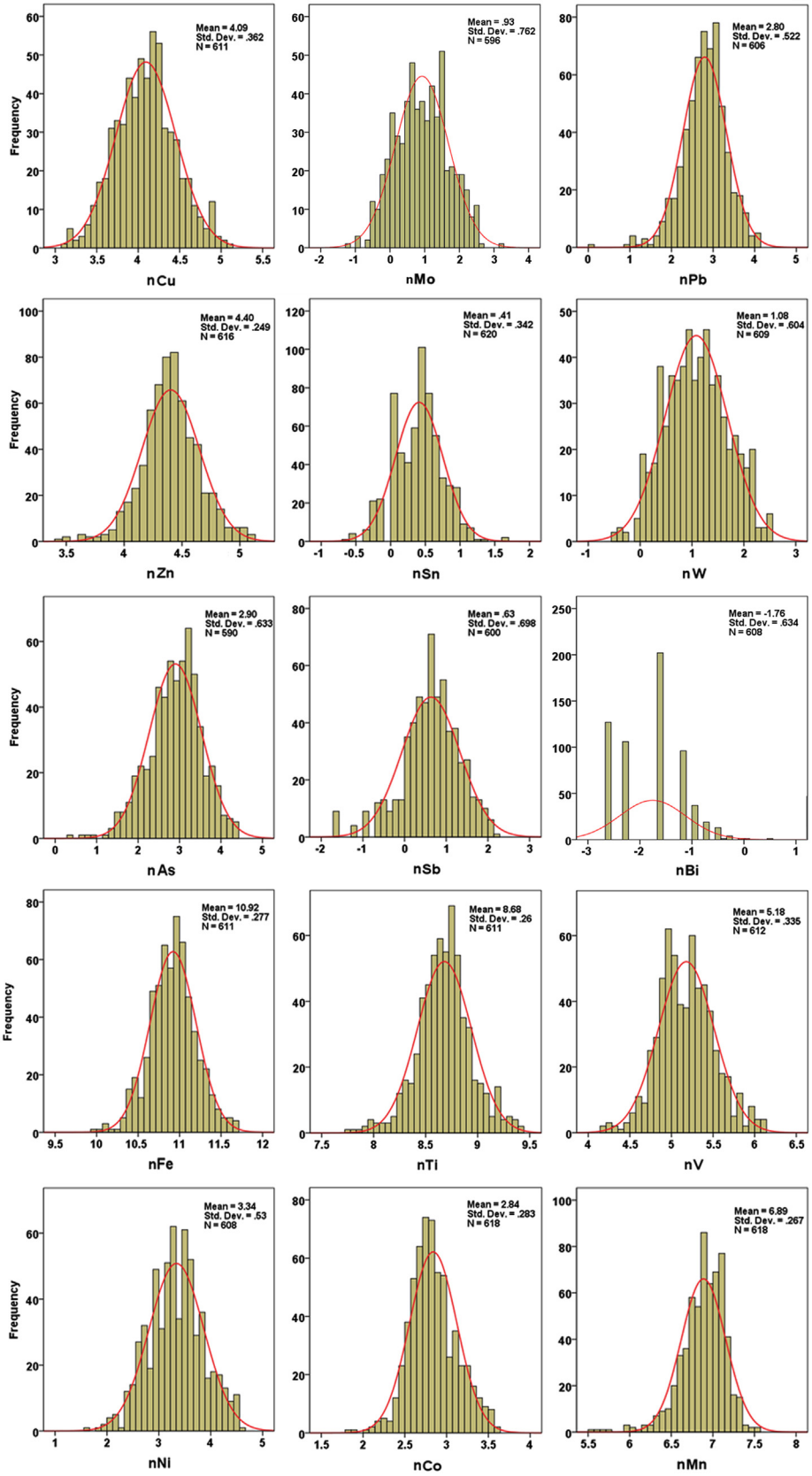

Fig. 6. Frequency histograms of the logarithmically normalized data after omitting the out of range samples.

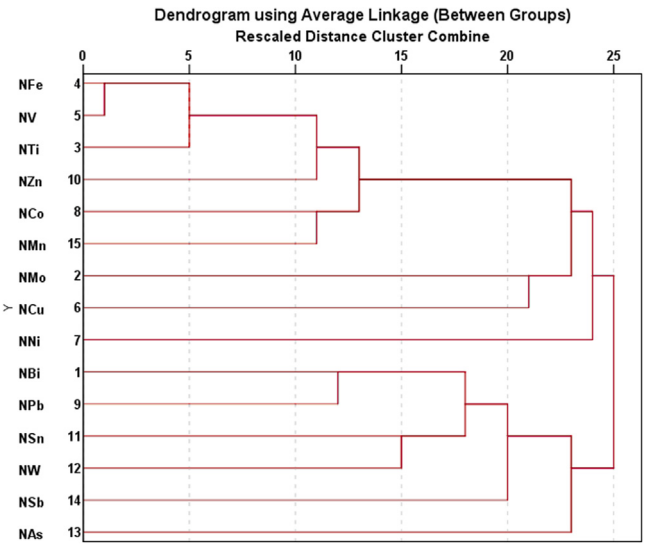

Fig. 7. Cluster dendrogtam of the selected elements, based on the logarithmically normalized data.

values, this model will display gradual variations from the background towards the threshold and anomaly values and will enhance the credibility of the anomaly.

4. Results and discussion

4.1. Element correlations

Based on the data shown in Table 3b and the Pearson correlation coefficient of normalized values at the 99% confidence level, the highest correlation exists among Ti, Fe and V with correlation coefficient greater than 0.70. Also good correlation exists between Co and Ni, as well as Fe, V and Mn (>0.0500). Additionally, Zn shows good correlation with Ti, Fe and V (~0.550). These may indicate a paragenetic relationship among these elements, especially their coexistence within mafic rocks. However, correlations between other pairs of elements are not statistically significant. The Spearman correlation coefficient was calculated using the raw data (Table 3a). Though the results of these two methods are occasionally different, especially when the number of out of range samples is high (Wellmer, 1998), comparing both results in this study shows that there is not a considerable difference between these two sets of results, implying their low affection by the out of range samples and the rather normal distribution of the elements. Similarly, the highest correlation exists among Ti, Fe and V (>0.700), while Co, Zn and Mn also show good correlation with these elements. Other remarkable correlations exist between W-Mo, W-Pb, W-Sn, W-Sb and W-Bi pairs of elements. Arsenic is in good correlation with Sb and Bi, and finally, Bi shows high correlation with Mo, Pb, Sn, W and As. These correlation coefficients may reflect paragenetic co-occurrence of these elements, which is supported by the presence of porphyry (Sonajil porphyry Cu prospect) and epithermal mineralizations (e.g., at Khankandi intrusive body), as well as other evidence found at NE and SE parts of the area during field control survey, which will be discussed later.

Based on the cluster dendrogram illustrated in Fig. 7, Fe, Ti, V, Co, Zn and Mn form a single group and Bi, Pb, Sn, W, Sb and As form another group, which may indicate the existence of paragenetic relationship among these variables.

4.2. Anomaly maps of the selected elements

Background, threshold and anomaly limits for the selected elements are calculated as: [> Mean + Standard deviation (Sd)], [Mean + 2Sd], and [>Mean + 2Sd], respectively, using the normalized data (Hassani Pak, 2012). Based on the calculated values and using the isochemical contour maps, distribution of each element and their anomaly zones were determined across the region. According to the obtained anomaly maps (Fig. 8), anomalies of the selected elements are as below:

4.2.1. Cu

Anomalies of this element show very good correlation with Oligocene granitic to granodioritic intrusions and the related hydrothermal alterations within Eocene andesitic-basaltic rocks at NE and central parts of the quadrangle, inasmuch as a major anomaly is formed at the location of the porphyry-type Cu mineralization at Sonajil and its surrounding hydrothermal alteration halos. High-grade epithermal gold veins, as well as many banded quartz, quartz-sulfide, quartz-oxide and sulfide veins and veinlets of various generations are developed within the microdioritic porphyry stock, portraying a distinct stock-work texture. Sulfide bearing veins are also found around the porphyry stock (Hosseinzadeh et al., 2010).

Additionally, NE part of the quadrangle contains silicic, advanced argillic and alunitic alterations and Cu and Au mineralization in the form of silicic veins (more than 18 veins with NW-SE trend, several cm up to 10 m thick and several m to several hundred m long), which are related to the intrusion of Khankandi and Yuseflu granitic-granodioritic intrusions into the volcanic rocks of Eocene age. Silicic veins contain pyrite, chalcopyrite, bornite, galena, sphalerite and molybdenite.

Another anomaly is related to the Razgah intrusion, where Cu mineralization has occurred as chalcopyrite and malachite. The highest Cu value within the stream sediments is 420 ppm.

4.2.2. Mo

Anomalies of Mo are more or less correlated with those of Cu, displaying very strong relationship with granitic to granodioritic intrusions of Oligocene age, especially at the northern part of the area, as well as with hydrothermal alterations within andesitic and trachy-andesitic rocks of Pliocene at the SE part of the quadrangle, which are attributed to the fumarolic activities. The highest concentration of Mo within the stream sediments is 3350 ppm.

4.2.3. Pb

Anomalies of Pb mainly and highly correspond with Oligocene granitic-granodioritic intrusions and the related hydrothermal alterations within Eocene andesitic-basaltic rocks. Two distinct anomalies also correlate with Sonajil and Razgah intrusive bodies, where Cu mineralization is evident. Another significant anomaly seems to be related to the hydrothermal alterations within hydrothermally altered (silicic and argillic) andesitic to trachy andesitic and basaltic rocks of Pliocene age at the SE part of the quadrangle, where silicic veins and veinlets containing Pb-Zn, Au and Cu mineralization were found. Among the rock samples taken during field control survey, 2 samples had relatively high Pb contents of about 0.39 and 0.28%.

4.2.4. Zn

Zinc shows dispersed and small anomalies across the region. Some of them are related to the granitic-granodioritic rocks in the northern half of the map, as well as in the Sonajil deposit. Some others correlate with hydrothermal alterations within Eocene and Pliocene volcanic rocks at NE and SE part of the quadrangle. It seems likely that the anomalous zone at the southeastern edge of the map, located downstream the rural areas, may be resulted by eco-environmental pollutions, for which more evidence and details will be presented and discussed below.

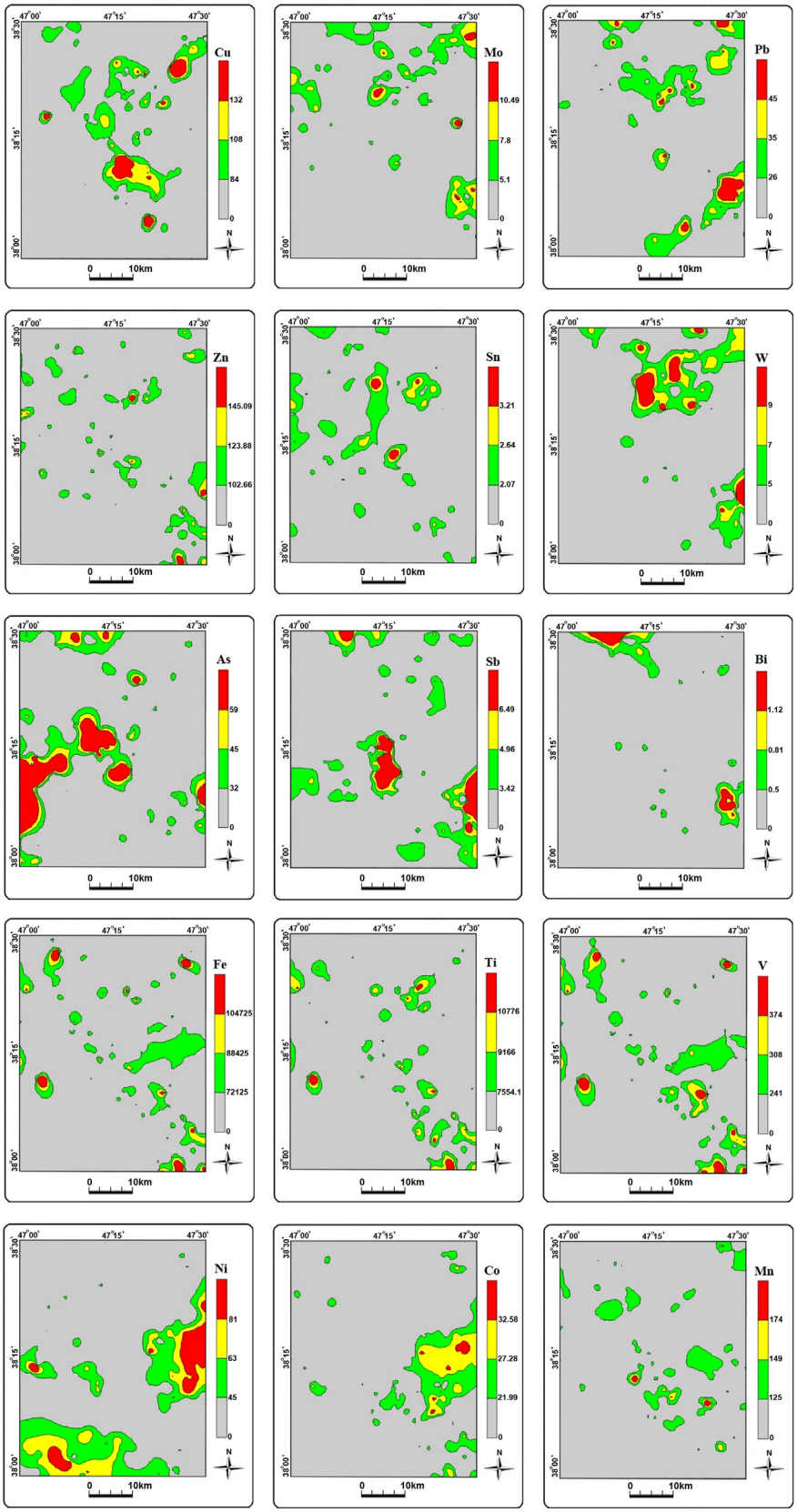

Fig. 8. Anomaly maps of the selected elements across the 1:100000 geologic map of Ahar.

4.2.5. Sn

The main anomalies of Sn correlate with granitic-granodioritic intrusions of Oligocene, for example in Sonajil, as well as with hydrothermal alterations within the volcanics of Eocene age.

4.2.6. W

The major anomalies of W show very well correlation with granitic intrusions at the NE part of the quadrangle and the related alterations within the Eocene volcanic rocks, as well as the alterations formed by volcanic fumaroles within Pliocene trachy-andesitic rocks.

4.2.7. As

One of the main As anomalous zones is located at the SW of the quadrangle, W and SW of Heris town. Lithology of this area is mainly comprised of gypsiferous marl, marliferous limestone, red conglomerate and marl of Miocene and Pliocene age, which are not favorable for producing such an anomaly. This anomaly may be produced by bio-environmental pollutions originated from the Heris town and the vast agricultural fields around it. Another zone is located at the center of the quadrangle, NE of Sonajil for which, following the streams upward and considering the fact that the next anomaly zone is related with the Sonajil intrusive body, it can be perceived that it may be created by streams originating from the Sonajil granitoid intrusion, which have transferred As to lower topographic levels.

4.2.8. Sb

Anomalies of Sb are found around the Sonajil porphyry copper prospect, and at the SE of the quadrangle, where epithermal Au and Pb-Zn silicic veins have been discovered, as well as at the NE of Ahar town, where the emplacement of the granitic-granodioritic intrusive body within the Paleocene and Eocene volcanics led to occurrence of fractures filled with silica veins and development of alteration zones. In this regard, a silicic vein is identified in this zone, 1–1.5 m thick and about 1 km long, which contains Fe-oxide, Pb, Zn, Cu and Au mineralization. This vein is located at the contact of the intrusive body with volcanic rocks. One rock sample taken during the field control survey displays relatively high concentrations of Pb (0.98%), Zn (0.19%), Cu (0.9%), Ag (334 ppm) and Au (850 ppb).

4.2.9. Bi

Anomalies of Bi correlate well with those of Mo, as well as with Cu in some extent. In general, they correspond with the granitic-granodioritic intrusion to the east of Ahar and the hydrothermal alterations formed within andesitic and trachy-andesitic rocks of Pliocene at the SE part of the Ahar quadrangle. Considering the presence of epithermal gold and Pb-Zn mineralization in these areas, it seems that Bi is also related to the epithermal processes. The highest concentration of Bi in the stream sediments is 5.2 ppm.

4.2.10. Fe

This element has scattered anomalies across the region. The one located at the NE corner of the quadrangle shows relationship with the Oligocene granitic-granodioritic intrusions, and those in the central parts of the map correlate with andesitic and basaltic rock of the Eocene age. However, some anomalies are located over areas covered by Quaternary alluvials, where there is no outcrop of the underlying rocks. In fact, these anomalies lie downstream the residential areas, such as SE of Ahar town (NW corner of the quadrangle), south of the Heris town (western part of the quadrangle), as well as the SE corner of the map, where several villages are located upstream. These anomalies may reflect bio-environmental (anthropogenic) pollutions. The highest yielded Fe concentration across the region is 25.6%.

4.2.11. Ti

Anomalies of Ti also display rather well correlation with those of Fe and V. Some of them are related with granitic-granodioritic intrusions of the Oligocene age (SE section of the quadrangle), as well as the Razgah intrusion (SE part of the quadrangle) and andesitic-basaltic volcanics of Eocene (central parts of the quadrangle). However, there are some anomalies at the neighborhood of urban and rural areas within the alluvial domains. The highest value measured for this element within the stream sediments is 4500 ppm.

4.2.12. V

It shows dispersed anomalies, highly correlating with the anomalies of Fe. Besides the anomalies at the eastern part of the map, which are related to the andesitic-basaltic rocks of Eocene and hydrothermal alteration zones within andesitic and trachy-andesitic rocks of Pliocene, other anomalies are located downstream the Ahar and Heris towns and the villages at the SE corner of the map, which similarly may reflect bio-environmental pollutions. The highest concentration of this element in stream sediments is 968 ppm.

4.2.13. Ni

This element shows a large anomalous zone at the eastern section of the map, correlating with the granitic-granodioritic intrusions of Oligocene age and the related hydrothermal alterations within the intermediate to mafic igneous rocks of Eocene and Pliocene. Another anomaly is located downstream the Sonajil intrusion and the related porphyry-type mineralization. All these anomalies indicate a paragenetic relationship between this element and the intrusive rocks in the region. Some dispersed anomalies are also present within the alluvial domains in the vicinity of residential areas, testifying to the likely bio-environmental pollutions caused by them. The highest measured Ni value is 221 ppm.

4.2.14. Co

The major anomaly zone of Co correlates with the volcanic rocks of Eocene and the hydrothermal alterations occurred within them, especially at the contact with Oligocene granitic body, east of the quadrangle. Another anomaly corresponds with granitoid intrusions at NE of the map. Some eco-environmental pollutions are also conceivable downstream the residential areas.

4.2.15. Mn

It shows insignificant and highly scattered anomalies across the region, mainly correlating with volcanic rocks of Paleocene and Eocene. An almost considerable anomaly is also found downstream the Sonajil intrusive body and the related mineralization.

5. Conclusion

In general, all the anomalies have good correlation with granitic-granodioritic intrusive bodies of Oligocene and the related hydrothermal alterations occurred within the Eocene andesitic-basaltic rocks, especially at NE part of the quadrangle, where vast hydrothermal alteration zones are formed including alunitic alteration, as well as alterations within trachy-andesitic and andesitic volcanics of Pliocene age at the SE part of the quadrangle, where vast alterations and also epithermal gold and Pb-Zn mineralization is found. The other source of base metal anomalies is the porphyritic intrusive body at Sonajil, which has brought about porphyry-type copper mineralization and hydrothermal alterations. Some anomalies also correlate with the Razgah monzosyenitic to foid-bearing monzosyenitic intrusion. Copper and to some extent Mo, as well

as Pb, Zn, Sn, W, As and Sb are the best examples of this relationship. However, As also shows a large anomaly zone downstream the Heris town and the agricultural fields south of it, most likely displaying a bio-environmental (anthropogenic) pollution. Bismuth has more limited anomalies across the area, showing correlation with granitoid intrusion at the east of Ahar and the hydrothermal alterations within the Pliocene andesitic and basaltic rocks at SE of Ahar quadrangle which, considering the presence of epithermal gold and Pb-Zn bearing silicic veins in both areas, can be attributed to epithermal processes.

Most of the anomalies of Fe, Ti and V show affiliation with andesitic-basaltic rocks of Eocene, though the role of granitic-granodioritic intrusions in producing anomalous zones is clearly evident. However, some anomalies are also observed downstream the urban and rural areas, which may have produced by bio-environmental pollutions. Ni, Co and Mn have almost similar situation. These relationships are also evident in calculation of correlation coefficients, as well as in the prepared dendrogram.

In this regard, besides the Sonajil area, where porphyry-type Cu mineralization is discovered, the NE part of the quadrangle presents a promising prospect to focus on for the detailed investigations, owing to the presence of silicic and advanced argillic alterations and Cu and Au mineralizations in the form of silicic veins containing high grades of Au (179–365 ppb in rock samples) and base metal sulfide minerals.

The southeastern part of the quadrangle also offers promising features, proposing further investigations, as the highest gold content in stream sediments (37.9 ppb) and rock (973 ppb) samples, as well as relatively high concentrations of Pb and Zn are obtained from this zone.

Acknowledgments

We thank the Geologic Survey of Iran-NW branch for funding and collaboration in this research. This work was carried out in the Department of Earth Sciences and Research Institute for Fundamental Sciences, University of Tabriz. Authors wish to thank Prof. Gültekin Topuz and Dr. Mansour Edraki for their constructive reviews and comments, which helped to improve the manuscript.

References

Agha Nabaty, E., 2004. Geology of Iran. Geological survey and mineral exploration organization of Iran, Tehran (in Persian).
Aghazadeh, M., Castro, A., Omran, N.R., Emami, M.H., Badrzadeh, Z., 2010. The gabbro (shoshonitic)-monzonite-granodiorite association of Khankandi pluton, Alborz mountains, NW Iran. Iran. J. Asian Earth Sci. 38, 199–219.
Aghazadeh, M., Castro, A., Badrzadeh, Z., Vogt, K., 2011. Post-collisional polycyclic plutonism from the Zagros hinterland: the Shaivar Dagh plutonic complex, Alborz belt, Iran. Geol. Mag. 148, 980–1008.
Alavi, S. Gh., Hosseinzadeh, M.R., Moayyed, M., 2014. Petrography and petrology of the Sungun porphyry copper deposit and post mineralization dykes with a view to skarn mineralization (north of Varzeghan, East Azarbaijan). Petrol 17, 17–32 (in Perisan).
Alavi, M., 1991. Sedimentary and structural characteristics of the paleo-tethys remnants in northeastern Iran. Geol. Soc. Am. Bull. 103, 983–992.
Alavi, M., 2004. Regional stratigraphy of the Zagros fold-thrust belt of Iran and its proforeland evolution. Am. J. Sci. 304, 1–20.
Allen, M.B., Armstrong, H.A., 2008. Arabia–Eurasia collision and the forcing of mid Cenozoic global cooling. Palaeogeogr. Palaeoclimatol Palaeoecol. 265, 52–58.
Axen, G.J., Lam, P.S., Grove, M., Stockli, D.F., Hassanzadeh, J., 2001. Exhumation of the west-central Alborz Mountains, Iran, Caspian subsidence, and collision-related tectonics. Geology 29, 559–562.
Berberian, M., King, G.C.P., 1981. Towards paleogeography and tectonic evolution of Iran. Can. J. Earth Sci. 18, 210–265.
Berberian, F., Muir, I.D., Pankhurst, R.J., Berberian, M., 1982. Late Cretaceous and early Miocene Andean type plutonic activity in northern Makran and Central Iran. J. Geol. Soc. London 139, 605–614.
Castro, A., Aghazadeh, M., Badrzadeh, Z., Chichorro, M., 2013. Late Eocene–Oligocene post-collisional monzonitic intrusions from the Alborz magmatic belt, NW Iran. An example of monzonite magma generation from a metasomatised mantle source. Lithos 180–181, 109–127.
Chork, C.Y., 1991. An assessment of least median of squares regression in exploration Geochemistry. J. Geochem. Explor. 41, 325–340.
Clark, I., 1987. Practical Geostatistics. Elsevier Applied Science Publishers Ltd, London, 129 p.
Cohen, D.R., Silva-Santisteban, C.M., Rutherford, N.F., Garnett, D.L., Waldron, H.M., 1999. Comparison of vegetation and stream sediment geochemical patterns in northeastern New South Wales. J. Geochem. Explor. 66, 469–489.
Dargahi, S., Arvin, M., Pan, Y., Babaei, A., 2010. Petrogenesis of post-collisional A-type granitoids from the Urumieh-Dokhtar magmatic assemblage, southwestern Kerman, Iran: constraints on the Arabian-Eurasian continental collision. Lithos 115, 190–204.
Fletcher, W.K., 1997. Stream sediment geochemistry in today's exploration world. In: Gubins, A.G. (Ed.), Proceedings of Exploration 97. Fourth Decennial International Conference on Mineral Exploration, pp. 249–260.
Ghorbani, M.R., Bezenjani, R.N., 2011. Slab partial melts from the metasomatizing agent to adakite, Tafresh Eocene volcanic rocks, Iran. Isl. Arc 20, 188–202.
Hale, M., Plant, J.A., 1994. Drainage geochemistry. In: Govett, G.J.S. (Ed.), Handbook of Exploration Geochemistry, Vol. 6. Elsevier.
Hassani Pak, A.A., Sharafaldin, M., 2005. Interpretation of Exploration Data. University of Tehran Publication, Tehran, 987 p. (in Persian).
Hassani Pak, A.A., 2012. Principles of Geochemical Exploration. University of Tehran Publication, Tehran, 615 p. (in Persian).
Hosseinzadeh, Gh., Calagari, A.A., Moayyed, M., Hadj-Alilu, B., Moazzen, M., 2010. Study of hypogene alteration and copper mineralization in Sonajil area (east of Herris, east Azarbaidjan). Geoscience 74, 3–12 (in Persian).
Jamali, H., Yaghubpour, A.M., Mehrabi, B., 2012. Relationship between Cu and Au mineralizations with different magmatic phases within Khankandi and Yuseflu intrusive bodies, east of Ahar. Iran. J. Crystal. Miner. 20, 547–564 (in Persian).
Levinson, A.A., 1980. Introduction to Exploration Geochemistry. Applied Publishing Ltd., Wilmette, Illinois, 924 p.
Mahdavi, M.A., Amini Fazl, A., 1988. 1:100000 Geologic Map of Ahar, Iran. Geological Survey of Iran, Tehran.
Mederer, J., Moritz, R., Zohrabyan, S., Vardanyan, A., Melkonyan, R., Ulianov, A., 2014. Base and precious metal mineralization in Middle Jurassic rocks of the Lesser Caucasus: A review of geology and metallogeny and new data from the Kapan, Alaverdi and Mehmana districts. Ore Geol. Rev. 58, 185–207.
Moritz, R., Rezeau, H., Ovtcharova, M., Tayan, R., Melkonyan, R., Hovakimyan, S., Ramazanov, V., Selby, D., Ulianov, A., Chiaradia, M., Putlitz, B., 2016. Long-lived, Stationary Magmatism and pulsed porphyry systems during Tethyan Subduction to post-collision evolution in the southernmost Lesser Caucasus, Armenia and Nakhitchevan. Gondwana Res. 37, 465–503.
Nabavy, H., 1976. An Introduction to the Geology of Iran. Geological Survey of Iran, Tehran, 109 p. (in Persian).
Nude, P.M., Arhin, E., 2009. Overbank sediments as appropriate geochemical sample media in regional stream sediment surveys for gold exploration in the Savannah regions of northern Ghana. J. Geochem. Explor. 103, 50–56.
Rantitsch, G., 2000. Application of fuzzy clusters to quantify lithological background concentrations in stream sediment geochemistry. J. Geochem. Explor. 71, 73–82.
Shahabpour, J., 2007. Island-arc affinity of the central Iranian volcanic belt. J. Asian Earth Sci. 30, 652–665.
Simmonds, V., 2013. Geochemistry and petrogenesis of an adakitic quartz monzonitic porphyry stock and related cross-cutting dyke suites Kighal, NW Iran. Inter. Geol. Rev. 55, 1126–1144.
Stocklin, J., 1974. Possible ancient con. In: ntal margins in, Iran., in Burk, C.A., Drake, C.L. (Eds.), The Geology of Continental Margins. Springer, Berlin, pp. 873–887.
Wellmer, F.W., 1998. Statistical Evaluations in Exploration for Mineral Deposits. Springer-Verlag, New York (379 p.).